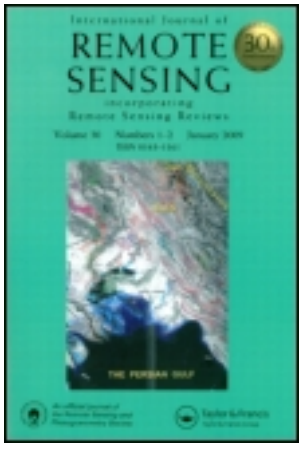

International Journal of Remote Sensing

Publication details, including instructions for authors and subscription information:
http://www.tandfonline.com/loi/tres20

Evaluation of detector-to-detector and mirror side differences for Terra MODIS reflective solar bands using simultaneous MISR observations

Aisheng Wu [a], Xiaoxiong Xiong [b], A. Angal [a] & W. Barnes [c]

[a] Science Systems and Applications, Inc., 10210 Greenbelt Road, Suite 600, Lanham, MD, 20706, USA

[b] Sciences Exploration Directorate, NASA/GSFC, Greenbelt, MD, 20771, USA

[c] University of Maryland, Baltimore County, Baltimore, MD, 21250, USA

Available online: 06 Feb 2011

To cite this article: Aisheng Wu, Xiaoxiong Xiong, A. Angal & W. Barnes (2011): Evaluation of detector-to-detector and mirror side differences for Terra MODIS reflective solar bands using simultaneous MISR observations, International Journal of Remote Sensing, 32:2, 299-312

To link to this article: http://dx.doi.org/10.1080/01431160903464138

International Journal of Remote Sensing
Vol. 32, No. 2, 20 January 2011, 299–312

Taylor & Francis
Taylor & Francis Group

Evaluation of detector-to-detector and mirror side differences for Terra MODIS reflective solar bands using simultaneous MISR observations

AISHENG WU*†, XIAOXIONG XIONG‡, A. ANGAL† and W. BARNES§
†Science Systems and Applications, Inc., 10210 Greenbelt Road, Suite 600, Lanham, MD 20706, USA
‡Sciences Exploration Directorate, NASA/GSFC, Greenbelt, MD 20771, USA
§University of Maryland, Baltimore County, Baltimore, MD 21250, USA

(*Received 30 September 2008; in final form 16 April 2009*)

The Moderate Resolution Imaging Spectroradiometer (MODIS) is one of the five Earth-observing instruments on-board the National Aeronautics and Space Administration (NASA) Earth-Observing System (EOS) Terra spacecraft, launched in December 1999. It has 36 spectral bands with wavelengths ranging from 0.41 to 14.4 μm and collects data at three nadir spatial resolutions: 0.25 km for 2 bands with 40 detectors each, 0.5 km for 5 bands with 20 detectors each and 1 km for the remaining 29 bands with 10 detectors each. MODIS bands are located on four separate focal plane assemblies (FPAs) according to their spectral wavelengths and aligned in the cross-track direction. Detectors of each spectral band are aligned in the along-track direction. MODIS makes observations using a two-sided paddle-wheel scan mirror. Its on-board calibrators (OBCs) for the reflective solar bands (RSBs) include a solar diffuser (SD), a solar diffuser stability monitor (SDSM) and a spectral-radiometric calibration assembly (SRCA). Calibration is performed for each band, detector, sub-sample (for sub-kilometre resolution bands) and mirror side. In this study, a ratio approach is applied to MODIS observed Earth scene reflectances to track the detector-to-detector and mirror side differences. Simultaneous observed reflectances from the Multi-angle Imaging Spectroradiometer (MISR), also onboard the Terra spacecraft, are used with MODIS observed reflectances in this ratio approach for four closely matched spectral bands. Results show that the detector-to-detector difference between two adjacent detectors within each spectral band is typically less than 0.2% and, depending on the wavelengths, the maximum difference among all detectors varies from 0.5% to 0.8%. The mirror side differences are found to be very small for all bands except for band 3 at 0.44 μm. This is the band with the shortest wavelength among the selected matching bands, showing a time-dependent increase for the mirror side difference. This study is part of the effort by the MODIS Characterization Support Team (MCST) in order to track the RSB on-orbit performance for MODIS collection 5 data products. To support MCST efforts for future data re-processing, this analysis will be extended to include more spectral bands and temporal coverage.

*Corresponding author. Email: aisheng.wu@sigmaspace.com

International Journal of Remote Sensing
ISSN 0143-1161 print/ISSN 1366-5901 online

http://www.tandf.co.uk/journals
DOI: 10.1080/01431160903464138

1. Introduction

The Moderate Resolution Imaging Spectroradiometer (MODIS) is one of the key instruments for the National Aeronautics and Space Administration's (NASA) Earth-Observing System (EOS) missions (Salomonson *et al.* 1989, Barnes and Salomonson 1993, Barnes *et al.* 2003). Its proto-flight model was launched on-board the Terra spacecraft on 18 December 1999 in a near Sun-synchronous descending polar orbit that crosses the equator at 10:30 a.m. local time. Since launch, it has been continuously providing global observations of the Earth's land, oceans and atmosphere and generating a broad range of science data products (Esaias *et al.* 1998, Justice *et al.* 1998, King *et al.* 2003, Moody *et al.* 2005). MODIS has 36 spectral bands with wavelengths from 0.41 to 14.4 μm and makes observations at three nadir spatial resolutions: 0.25, 0.5 and 1 km. MODIS bands are located on four focal plane assemblies (FPAs): the visible (VIS), near infrared (NIR), short-wave and mid-wave infrared (SW/MWIR) and long-wave infrared (LWIR) FPA, aligned in the cross-track direction. For each 0.25, 0.5 and 1 km band, there are 40, 20 and 10 detectors, respectively. The detectors in each spectral band are aligned in the along-track direction. MODIS collects data using a two-sided paddle-wheel scan mirror. The rotation of the scan mirror allows continuous measurements to be made from the on-board calibrators (OBCs) and the underlying Earth scenes. The scan angle range of the Earth view is between $+55^\circ$ and -55° from the instrument nadir, which covers a swath of 10-km (nadir) along-track by 2330-km cross-track each scan.

MODIS OBCs include a solar diffuser (SD), a solar diffuser stability monitor (SDSM), a spectral-radiometric calibration assembly (SRCA), a blackbody (BB) and a space view (SV) port that provides a clear view of dark space for measuring instrument background and detector offsets. SD/SDSM calibration data have shown that the Terra MODIS system response in the visible spectral region has a significant wavelength dependent degradation over time (Guenther *et al.* 2002, Xiong *et al.* 2002b, 2003a,b, 2007, Xiong and Barnes 2006). After more than 7 years of on-orbit operation, detector responses have changed by 20%, 15%, 3% and 1% for the spectral bands at wavelengths of 0.47 μm (band 3), 0.56 μm (band 4), 0.65 μm (band 1) and 0.85 μm (band 2), respectively. The SD calibration is performed at a scan mirror angle of incidence (AOI) of 50.2°. Comparison of the SD calibration results with response trending from SRCA (AOI = 38.0°) and lunar observations (AOI = 11.2°) shows that the optical degradation is AOI dependent. In addition, the degradation rates between the two sides of the scan mirror are different, with mirror side 2 degrading faster than side 1 (Xiong *et al.* 2002b, 2003a, Sun *et al.* 2003, 2007, Xiong and Barnes 2006).

MODIS OBC data are collected at a fixed AOI with well characterized source targets. In order to study MODIS performance over its complete AOI range between 10.5° and 65.5°, it is necessary to use the Earth view observations. However, the scene-associated variations, such as those due to the occurrence of clouds and vegetation, complicate the direct use of scene observations. In order to reduce the impact due to scene variations, it is helpful to use observations over relatively homogeneous surface targets such as deserts and oceans (Thome *et al.* 1997, Rao and Chen 1999). An alternative approach is to use another sensor, serving as a transfer radiometer, for reference to track the sensor performance (Cao and Heidinger 2002, Wu *et al.* 2003, 2008, Xiong *et al.* 2008b). The advantage of this approach is that it can significantly reduce the impact of scene-associated variations if observations from both sensors match well in terms of temporal, spatial and spectral characteristics.

Also on-board the Terra spacecraft are the Advanced Spaceborne Thermal Emission and Reflection Radiometer (ASTER), Clouds and the Earth's Radiant Energy System (CERES), Multi-angle Imaging Spectroradiometer (MISR) and Measurements of Pollution in the Troposphere (MOPITT) (King and Greenstone 1999). In this study, we use MISR to help characterize MODIS reflector solar band (RSB) detector-to-detector and mirror side differences. MISR has nine cameras, each with four reflective solar spectral bands (RSBs), which are closely matched to MODIS bands 1–4 (Diner *et al.* 1998). The MISR cameras are off-set from one another in a push-broom configuration, enabling observations to be made at a broad range of angles in the track direction. MISR nadir camera data are collected near simultaneously with MODIS data, in a narrow swath of 370 km.

In this study, a ratio approach is applied to co-located MODIS and MISR pixel pairs obtained from near-simultaneous Earth scene observations. This approach determines MODIS relative detector-to-detector and mirror-side differences with the help of MISR. It focuses on MODIS nadir observations at an AOI of 38.0°, due to a narrow MISR swath. The results of this study provide a direct assessment of the calibration impact on MODIS nadir observations in the current version 5 Level 1 B (L1B) RSB data products, which are determined from the SD and lunar observations obtained at two different AOIs.

2. MODIS and MISR instrument calibration

2.1 *MODIS*

MODIS's 36 spectral bands are distributed on four separate focal plane assembles with central wavelengths from 0.41 to 0.55 μm on the visible (VIS) focal plane, 0.64 to 0.94 μm on the NIR focal plane, 1.20 to 2.30 μm and 3.60 to 4.50 μm on the SW/MWIR focal plane and 6.50 to 14.40 μm on the LWIR focal plane. The calibration of these bands is based on on-board measurements from the SD, SDSM, SRCA and BB. Instrument background signals are provided by the detector's view of deep space through the SV port and removed from measured total detector responses. Bands 1–19 and 26 with spectral wavelengths from 0.41 to 2.2 μm are the RSBs and are calibrated by the SD and SDSM. The SD is a flat plate of space grade Spectralon®, which acts as a near-Lambertian reflector. During the SD calibration period, the SDSM alternately measures reflected light off the SD and direct solar irradiance to monitor the SD degradation. The SRCA is primarily used for all band spatial characterization through band-to-band registration and for RSB spectral characterization and radiometric stability monitoring. The BB provides a scan-by-scan calibration of the thermal emissive bands (TEB), based on a temperature controlled blackbody (Xiong *et al.* 2002a).

Based on calibration measurements from the SD/SDSM, the reflectance factor $\rho_{EV}\cos(\theta_{EV})$ is given by

$$\rho_{EV}\cos(\theta_{EV}) = m_1 C_{EV} d_{ES}^2 (1 + k_{inst}\Delta T)/R_{EV} \quad (1)$$

where θ_{EV} is the Earth view (EV) solar zenith angle, m_1 is the calibration coefficient determined from the SD/SDSM measurements, C_{EV} is the detector response to the top-of-the-atmosphere radiance, d_{ES} is the Earth–Sun distance in AUs (astronomical units), k_{inst} is the instrument temperature correction coefficient (Xiong *et al.* 2006), ΔT is the difference of the instrument temperature from its reference value and R_{EV} is the response

versus scan angle at the EV AOI. The k_{inst} coefficient values are based on pre-launch thermal vacuum tests, in which the instrument is set at different temperatures in order to evaluate the impact of changes in instrument temperature. Values of R_{EV} are referenced to the value at the SD AOI of 50.2°, and the change of the R_{EV} as a function of AOI is determined based on the response differences between the SD and lunar (11.2°) AOI.

2.2 *MISR*

MISR observes the Earth's surface simultaneously at nine widely separated angles, at and off nadir, in the along-track direction (Diner *et al.* 1998, 2002). MISR has four RSBs at blue, red, green and near-infrared wavelengths with a resolution of 275 m at nadir. Its central wavelength and effective bandwidths are compatible to four MODIS bands, as listed in table 1.

The MISR calibration is provided by its on-board calibrators (M-OBCs) and vicarious calibration experiments conducted using desert targets in the southwestern United States (Bruegge *et al.* 1993, Chrien *et al.* 2002, Bruegge *et al*. 2007). The M-OBCs consist of two Spectralon diffuse panels and six sets of photodiode detectors, which are used to measure incoming and reflected solar irradiance from the panels. These measurements are regressed against the camera's digital output to provide the MISR radiometric calibration for each of the 1504 charged-coupled device (CCD) detector elements in each band. It is believed that MISR prelaunch tests might not adequately account for the out-of-band spectral response. So the absolute radiometric calibration at launch is a big concern. However, MISR observed EV trending results suggest M-OBC calibration data provide accurate camera-relative, band-relative and pixel-to-pixel calibrations (Abdou *et al.* 2002). Due to uncertainties with the M-OBC absolute calibration, periodic vicarious calibration experiments are conducted to adjust the calibration of the nadir camera (Bruegge *et al.* 1998, Chrien *et al.* 2002, Bruegge *et al*. 2007).

3. Methodology

3.1 *Pixel-by-pixel co-location*

Each MISR scene can be co-located with a MODIS near nadir scene since MISR and MODIS are on the same platform with a similar viewing geometry (figure 1). A MISR data granule includes the four spectral bands for the entire daylight side of the Earth over a single orbit. There is a separate granule for each of the nine cameras. The data

Table 1. Moderate Resolution Imaging Spectroradiometer (MODIS) and Multi-angle Imaging Spectroradiometer (MISR) spectrally-matched band parameters.

MODIS			MISR		
λ_c (μm)	$\Delta\lambda$ (μm)	Band	λ_c (μm)	$\Delta\lambda$ (μm)	Band
0.469	0.020	3	0.446	0.041	Blue
0.555	0.020	4	0.558	0.027	Green
0.645	0.050	1	0.672	0.020	Red
0.858	0.035	2	0.867	0.038	Near-infrared

Note: λ_c is the central wavelength and $\Delta\lambda$ is the bandwidth.

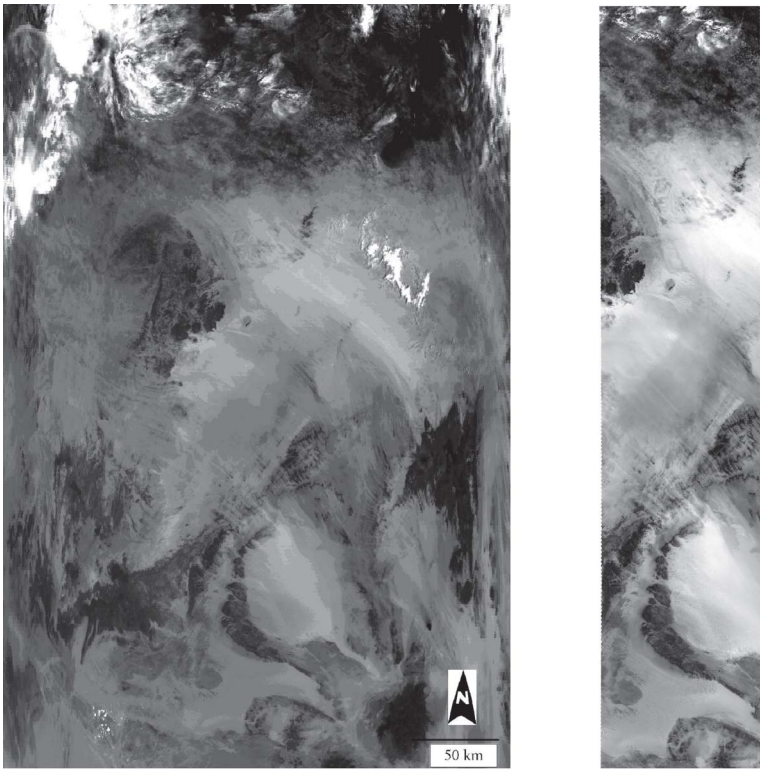

(*a*) (*b*)

Figure 1. An example of simultaneous observations of the 0.6 μm bands over the northern African region (13.5–31.6° N, 0.0–22.0° E) at 10:00 (Greenwich Mean Time, GMT) on 12 September 2000 from (*a*) the Moderate Resolution Imaging Spectroradiometer (MODIS) and (*b*) the Multi-angle Imaging Spectroradiometer (MISR) of the Terra platform. The overlapping area of the MODIS and MISR observations is in the middle portion of the MODIS image.

files for the nadir camera (AN files) are provided in the Georectified Radiance Product (GRP). There are two kinds of GRP AN files: Ellipsoid-projected and Terrain-projected. The difference between Ellipsoid and Terrain GRP radiances is in the altitude data used at each location on the grid. In the Ellipsoid product, the altitude is represented by the WGS84 ellipsoid. The Terrain product uses the altitude of the Earth's terrain. All MISR granules use a special form of the Hierarchical Data Format - Earth Observing System (HDF-EOS) grid format called the stacked block format. They are divided into 180 blocks, each being 370 km in the cross-track dimension by 140 km in the along-track dimension. This study uses AN datasets at a reduced resolution of 1.1 km (also called reduced AN pixels). Further details on the MISR data product are available from the MISR website, http://www-misr.jpl.nasa.gov/mission/pub.html.

Unlike a MISR granule, which covers a single orbit, a MODIS granule is limited to a 5-minute interval containing only 203 scans in the along-track direction, corresponding to a distance of 2330 km. To collect co-located MODIS and MISR pixels, MISR blocks overlapping with MODIS scans are extracted. To make sure that

consistent datasets are used from both MODIS and MISR observations, all MODIS granules are from the Version-5 L1B product and all MISR granules are from a single version number (F03-024).

For a MISR pixel with a longitude $X_{\mathrm{MISR}}(i, j)$ and a latitude $Y_{\mathrm{MISR}}(i, j)$ and a MODIS pixel with a longitude $X_{\mathrm{MODIS}}(k, l)$ and a latitude $Y_{\mathrm{MODIS}}(k, l)$, the distance between the two pixels can be expressed as

$$d = \sqrt{\left[X_{\mathrm{MISR}}(i,j) - X_{\mathrm{MODIS}}(k,l)^2 + [Y_{\mathrm{MISR}}(i,j) - Y_{\mathrm{MODIS}}(k,l)]\right]^2} \quad (2)$$

where i and j are the cross-track and along-track indices for a 1.1-km MISR block data file, and k and l are the cross-track and along-track indices for a 1-km MODIS granule data file. We can control the quality of pixel match-up co-location by selection of the minimum allowed value of d. Smaller values for d correspond to larger areas of overlap between the MODIS and MISR pixel pair. A value of d equals to 0.0025° (corresponding to a distance of 250 m between the centres of two pixels) is used in equation (2). With this restriction, approximately 10% of the total overlapping data points are matched.

3.2 *MODIS to MISR ratio*

In this study, the four MODIS bands (1 to 4) that are spectrally matched with the four MISR bands, as shown in table 1, are used. For each co-located MODIS and MISR pixel pair, a ratio of reflectance between MODIS and MISR, r, is calculated by

$$r_n(b,d,m) = \rho_n^{\mathrm{MODIS}}(b,d,m)/\rho_n^{\mathrm{MISR}}(b) \quad (n = 1, 2, 3, \ \ldots, \ N) \quad (3)$$

where N is the total number of matched pixel pairs extracted from each overpass. For MODIS, the reflectance of a 1-km pixel is determined for each band b, detector d and mirror side m. For MISR, the reflectance of a 1.1-km pixel is only dependent on band.

MODIS detector-to-detector difference ΔD is determined by

$$\Delta D(b,d) = \langle r_n(b,d,m)\rangle_{n,m} \Big/ \langle r_n(b,d,m)\rangle_{n,m,d} \quad (4)$$

MODIS mirror side difference ΔM is determined by

$$\Delta M(b) = \langle r_n(b,d,m)\rangle_{n,d,m=2} \Big/ \langle r_n(b,d,m)\rangle_{n,d,m=1} \quad (5)$$

where $\langle \ldots \rangle_{n,m}$ is the average of all available points at both mirror sides for each MODIS detector, $\langle \ldots \rangle_{n,m,d}$ is the average over all available points at both mirror sides of all MODIS detectors, and $\langle \ldots \rangle_{n,d,m=1}$ and $\langle \ldots \rangle_{n,d,m=2}$ are the average over all available points of all MODIS detectors at mirror sides 1 and 2, respectively.

4. Results

4.1 *MODIS detector-to-detector differences*

This study focuses on MODIS 1-km pixels, as they are used in most L1B data products. Thus, for MODIS bands 1 and 2 (0.25-km resolution, 40 detectors), detector '1' is actually the average of detectors 1–4 (MODIS Level 1 B 1-km product), detector '2' is the average of detectors 5–8 and so on. For MODIS bands 3 and 4 (0.50-km resolution, 20 detectors), detector '1' is the average of detectors 1 and 2, detector

'2' is the average of detectors 3 and 4 and so on. For the corresponding MISR bands, each 1.1-km pixel is an average of 4 × 4 275-m pixels.

Values of ΔD determined by equation (4) are used to examine detector-to-detector differences. If values of ΔD are close to 1.0 for all detectors, there are no detector-to-detector differences. Observations collected over the North African desert region are used to examine MODIS detector-to-detector differences. The location of these observations is not fixed at a specified geolocation but confined to be within the Libyan to Sudan Desert region. The advantage of using this desert region is that it provides a relative uniform and stable surface with high reflectance. Historic reflectance trends observed over the same area are used for vicarious calibration for sensors such as the National Oceanic and Atmospheric Administration (NOAA) series of AVHRR (Advanced Very High Resolution Radiometer), due to a lack of onboard calibrators. Figure 2 plots the normalized ratios versus detector number for bands 1 to 4 after averaging sampled pixels from multiple overpasses over the desert region from 2000 to 2007. There is a general decline in the ratios as the detector number increases, indicating a possible calibration bias. The variation between adjacent detectors (i.e. from one scan line to the next) is within 0.2%. The maximum relative difference between detectors 1 and 10 ranges from 0.5% to 0.8%, which appears to be dependent on band wavelength, with shorter wavelength bands showing larger relative detector difference. This is consistent with wavelength-dependent degradation trends found at

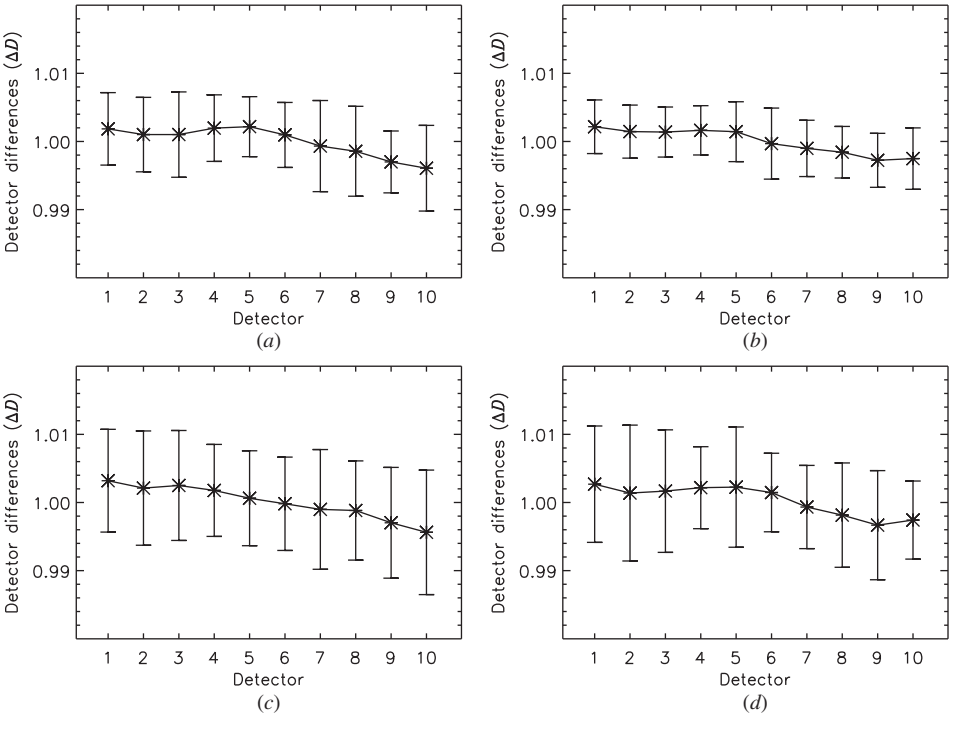

Figure 2. MODIS relative detector-to-detector differences ΔD in (*a*) band 1, (*b*) band 2, (*c*) band 3, (*d*) band 4. Results are obtained by averaging multiple overpasses over the North African desert region from years 2000 to 2007. Also shown is the range of the standard error (1 sigma).

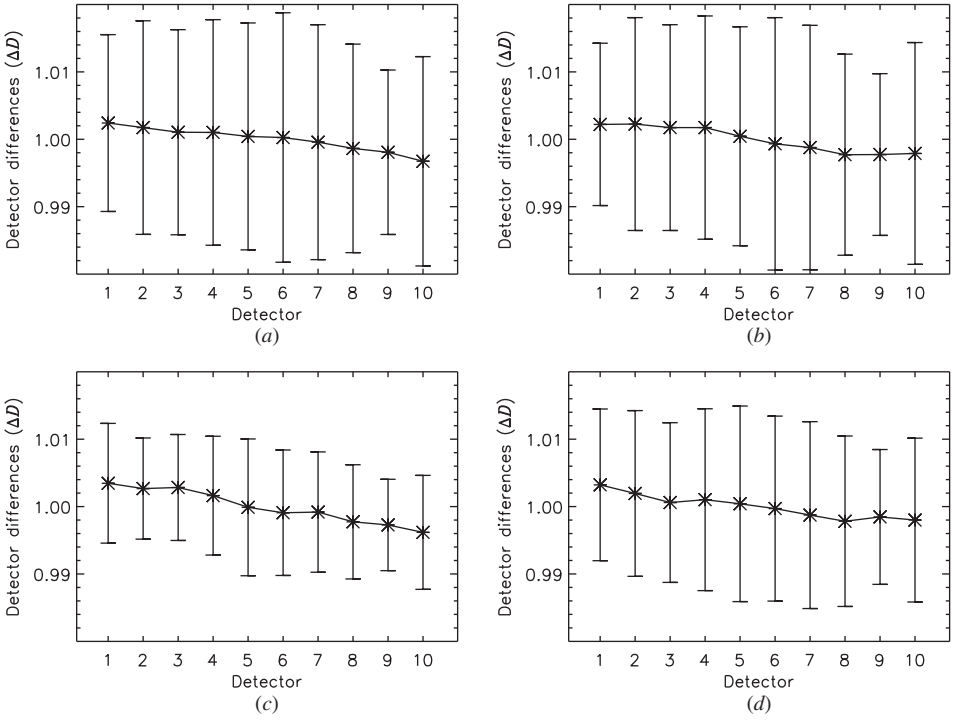

Figure 3. Same as figure 2, except the results are re-calculated by removing the ρ^{MISR} term applied in equation (3).

the system level for detector response; there is more degradation in shorter wavelength bands than in longer wavelength bands. Error bars (1 sigma) are determined from all sampled ΔD. To justify our current ratio approach as applied to MODIS and MISR reflectances, values of ΔD are re-calculated using MODIS measurements only. This is achieved by removing the term ρ^{MISR} used in equation (3). Results of the re-calculated ΔD are shown in figure 3. A comparison of the results of figures 2 and 3 shows that the error bars without MISR measurements are significantly larger, confirming the benefit of the ratio approach in reducing the variations in the ΔD results. The good agreement of ΔD results for the cases with and without MISR measurements justifies the approach of the direct use of MODIS Earth view observations for other AOIs beyond the nadir. Figure 4 shows the yearly trending results of the detector-to-detector difference since the launch of the instrument for each of the four bands. There is no significant relative change in ΔD among all 10 detectors over 7 years, confirming the stability of the calibration of each detector.

The existing small but noticeable detector-to-detector differences carried since the launch of the MODIS instrument are considered to be caused by a systematic calibration bias due to the use of the SD. The SD is made of pressed polytetrafluoroethylene. The bi-directional reflectance distribution (BRD) of the SD is the primary calibration component and any on-orbit SD reflectance degradation is tracked by the SDSM. The SD BRD was measured during prelaunch tests, while the on-orbit validation of the BRD was performed through a relative comparison early in the mission using spacecraft yaw manoeuvres. Since the yaw BRD results agree well with those obtained from

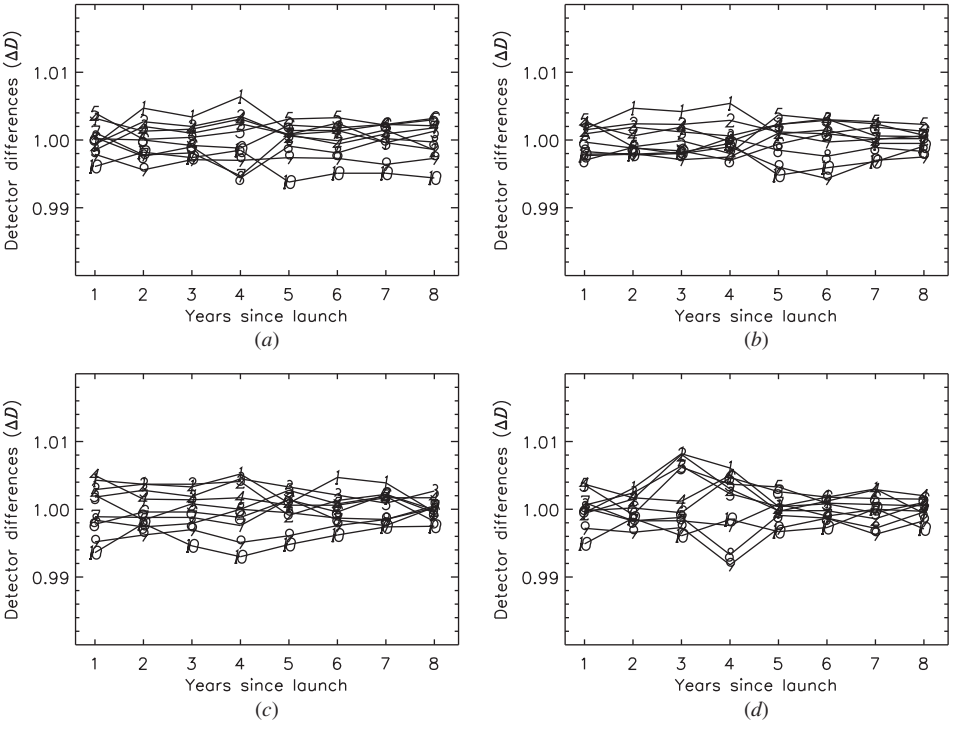

Figure 4. Yearly trends of the Moderate Resolution Imaging Spectroradiometer (MODIS) relative detector-to-detector differences ΔD in (*a*) band 1, (*b*) band 2, (*c*) band 3, (*d*) band 4 from 2000 to 2007. The numbers used represent each detector.

prelaunch tests, no on-orbit SD BRD adjustment has been applied. However, the SD door was fixed in the open position since 2 July 2003 leading to an increased rate of degradation of the SD. No yaw manoeuvres have been performed after the SD door anomaly to further validate the results obtained from the previous yaw manoeuvres. This study is part of the effort by the MODIS Characterization Support Team (MCST) in order to track the detector performance for MODIS collection 5 data products. To support future MCST data re-processing, this analysis will be extended to include more spectral bands and temporal coverage.

The current ratio approach used to examine MODIS detector differences is based on the assumption that MISR pixel-relative calibration is stable. Measurements from M-OBC show that MISR pixel-relative calibration differences are maintained to be within 0.5% (Bruegge *et al.* 1998, 2002). Since MISR pixel-relative differences are considered to be a random source of uncertainty, the use of 4×4 pixel averaging further reduces their pixel-relative uncertainties, which are estimated to be around only 0.2% (Bruegge *et al.* 1998). Thus, MISR pixel-relative uncertainties should have a negligible impact on the calculation of MODIS detector-to-detector differences. Our studies from highly reflective snow surfaces, such as the Dome C site in Antarctica, also show similar results (Xiong *et al.* 2008c). For the highly absorbing water surface, the visible band signals become extremely small and the results are less stable.

4.2 *MODIS mirror side reflectance ratio*

By separating MODIS/MISR reflectance ratios between the two MODIS mirror sides with no separation among detectors and then taking a ratio between the two (equation (5)) gives us the ratio of the reflectance of MODIS mirror side 1 to mirror side 2. Since MISR uses common optics for the adjacent observations, this ratio approach should have little impact on the MODIS mirror side ratio, while removing most scene variations. This approach is effective for the MODIS bands that are matched spectrally with the MISR bands. The small reflectance difference due to existing mismatch of MODIS and MISR spectral response functions is cancelled in this ratio approach. Figure 5 shows trending results of the MODIS mirror side reflectance ratios for bands 1 to 4. These results show that the ratios are within 0.2% of 1.0 for all bands except for band 3 at 0.446 μm (the shortest wavelength band of the four) near the end of the trending period, where the ratio shows a seasonally-related fluctuation of 0.5% to 1.0% after 2006 (after day 2500).

Although such fluctuations in the mirror side reflectance ratio are still well within the 2% calibration uncertainty reported previously (Esposito *et al.* 2004), it is unlikely that this is caused by the SD/SDSM calibration. Examination of the trending results of m_1 (equation (1)) obtained at the SD AOI of 50.2° shows that the gain ($1/m_1$) of band 3 decreases by 25%, compared with a decrease of 15% for band 4 and a small change of only 3% for band 1 (figure 6). The MODIS gain is proportional to the

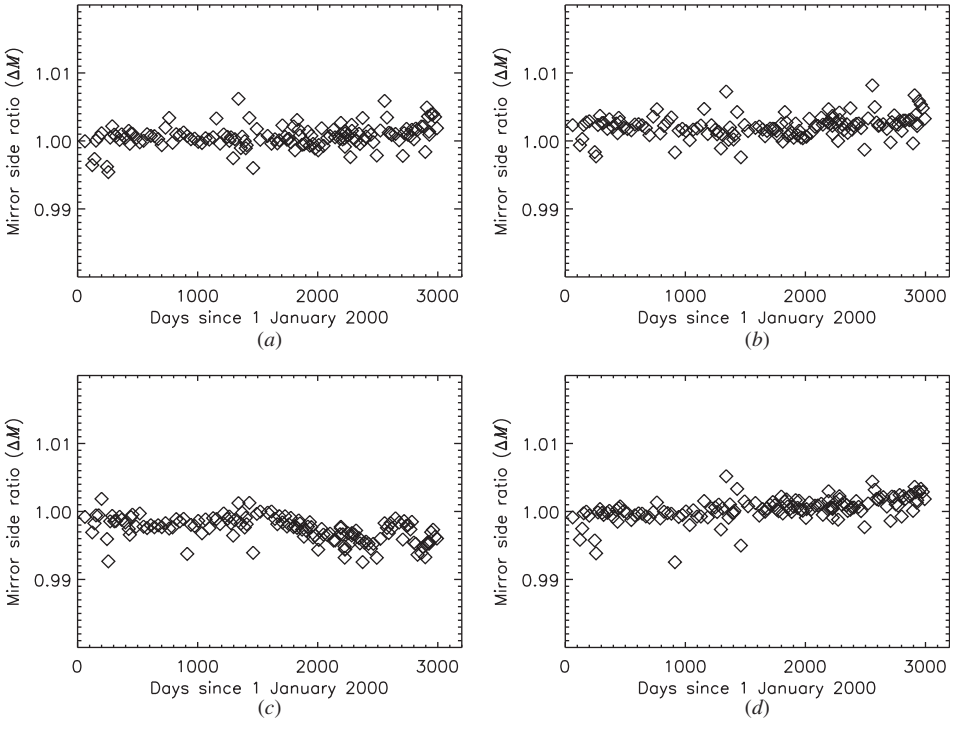

Figure 5. Trends of MODIS mirror side reflectance ratios ΔM (reflectance of mirror side 2 divided by mirror side 1) obtained from observations over the North African desert region for (*a*) band 1, (*b*) band 2, (*c*) band 3, (*d*) band 4.

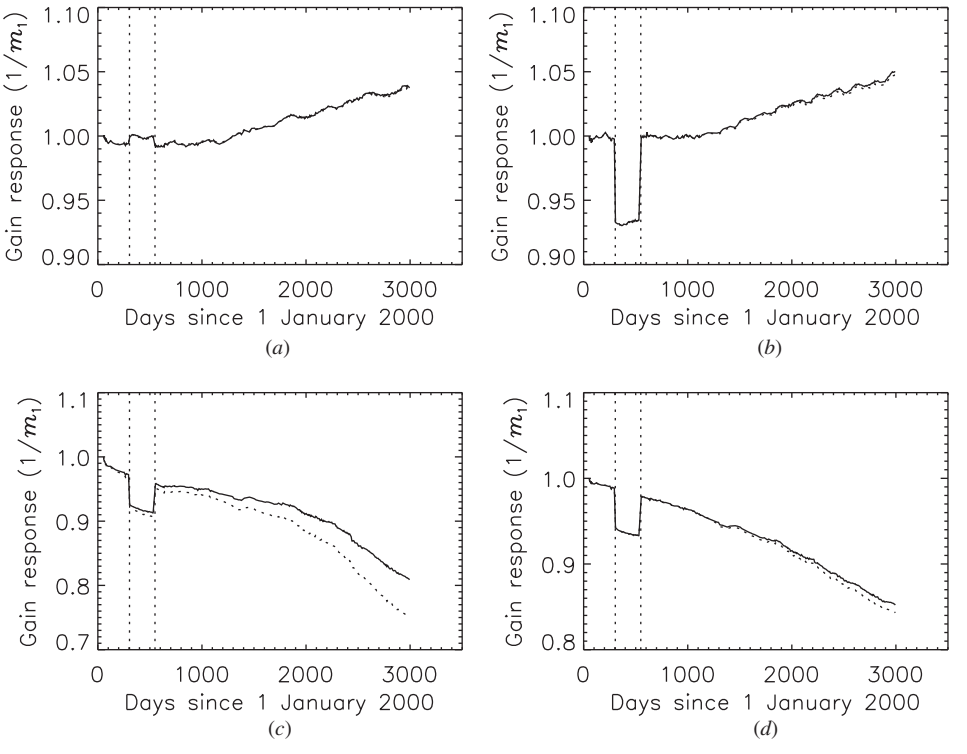

Figure 6. Trends of gain response $1/m_1$ for the Moderate Resolution Imaging Spectroradiometer (MODIS) band 1 (*a*), band 2 (*b*), band 3 (*c*) and band 4 (*d*). The solid line is for mirror side 1 and the dotted line for mirror side 2. The two vertical lines correspond to the times of two major changes in the instrument electronic configuration.

mirror reflectance, aft optics transmission, detector efficiency and electronic amplification. Previous studies have shown that the MODIS VIS/NIR degradation is primarily due to changes in mirror reflectance. Since the mirror reflectance is wavelength and AOI dependent, its change also shows similar dependency (Xiong *et al.* 2002b, 2007, 2008a). The mirror side difference in Terra MODIS (very small in Aqua MODIS) is likely due to the mirror contamination (not the same on both sides) and occurred during sensor pre-launch characterization (Kwiatkowska *et al.* 2008). It is also noted that the differences in m_1 between the two mirror sides are wavelength dependent with larger differences at shorter wavelengths. However, no seasonally related fluctuations occur for either trends of m_1 for each mirror side or the ratio of m_1 between the two mirror sides. Given the fact that there is a significant drop in gain response for bands with wavelengths ranging from 0.4 to 0.5 μm, other factors such as polarization may affect radiance/reflectance products. Currently, polarization corrections have not been applied in the MODIS RSB calibration scheme.

5. Summary

Calibration of the MODIS RSBs is performed for each band, detector and mirror side based on on-board measurements using the SD/SDSM. Historic calibration trending results indicate that the rate of the RSB degradation is not only wavelength-

dependent, but is also different between the two sides of the scan mirror. Comparisons of the calibration results from the SD/SDSM, SRCA and lunar observations show that the degradation rate also changes with the AOI.

This study uses MODIS observed Earth scene reflectances to determine the detector-to-detector and mirror side differences. To reduce the effects of scene variations, a ratio approach based on co-located MODIS and MISR pixel pairs, obtained from near-simultaneous overpasses, is used. Results show that adjacent detector-to-detector differences are less than 0.2% and the maximum differences between edge detectors range from 0.5% to 0.8%, depending on the band, indicating a possible calibration bias. The differences between the two mirror sides are extremely small. For MODIS band 3 at 0.446 μm, the shortest wavelength band among the four MODIS and MISR spectrally matching bands, results indicate that the mirror side ratio shows a seasonally-related fluctuation of about 1% after year 2006.

The results of this study demonstrate that a ratio approach applied to Earth scene observations is able to reduce most scene-associated variations occurring in the dataset. This allows us to study MODIS in-band detector quality, biases and mirror side differences. Another important aspect of combining MISR observations is to provide an evaluation of the calibration at the nadir AOI, which is determined based on calibration results obtained from two off nadir AOI angles used for SD and lunar observations.

Acknowledgements

The authors wish to acknowledge the useful clarifications by Brian Wenny and helpful grammatical corrections by Jennifer Dodd made to the manuscript. Both of them are from the MODIS Characterization Support Team.

References

Abdou, W., Bruegge, C., Helmlinger, M., Conel, J., Pilorz, S. and Caitley, B., 2002, Vicarious calibration experience in support of the Multi-angle Imaging SpectroRadiometer (MISR). *IEEE Transactions on Geoscience and Remote Sensing*, **40**, pp. 1500–1511.

Barnes, W.L. and Salomonson, V.V., 1993, MODIS: a global imaging spectroradiometer for the Earth Observing System. *Critical Review of Optical Science and Technology*, **47**, pp. 285–307.

Barnes, W.L., Xiong, X. and Salomonson, V.V., 2003, Status of Terra MODIS and Aqua MODIS. *Journal of Advances in Space Research*, **32**, pp. 2099–2106.

Bruegge, C., Chrien, N., Ando, R., Diner, D., Abdou, W., Helmlinger, M., Pilorz, S. and Thome, K., 2002, Early validation of the Multiangle Imaging SpectroRadiometer (MISR) radiometric scale. *IEEE Transactions on Geoscience and Remote Sensing*, **40**, pp. 1477–1492.

Bruegge, C., Chrien, N., Diner, D., Kahn, R. and Martonchik, J., 1998, MISR radiometric uncertainty analyses and their utilization within geophysical retrievals. *Metrologia*, **35**, pp. 571–579.

Bruegge, C., Diner, D., Kahn, R., Chrien, N., Helmlinger, M., Gaitley, B. and Abdou, W., 2007, The MISR radiometric calibration process. *Remote Sensing of Environment*, **107**, pp. 2–11.

Bruegge, C., Stiegman, A., Rainen, R. and Springsteen, A., 1993, Use of Spectralon as a diffuse reflectance standard for in-flight calibration of Earth-orbiting sensors. *Optical Engineering*, **32**, pp. 805–814.

Cao, C. and Heidinger, A., 2002, Inter-comparison of the longwave infrared channels of MODIS and AVHRR/NOAA-16 using simultaneous nadir observations at orbit intersections. *Proceedings of SPIE – Earth Observing Systems VII*, **4814**, pp. 306–316.

Chrien, N., Bruegge, C. and Ando, R., 2002, Multi-angle Imaging SpectroRadiometer (MISR) on-board calibrator (OBC) in-flight performance studies. *IEEE Transactions on Geoscience and Remote Sensing*, **40**, pp. 1493–1499.

Diner, N.L., Beckert, J.C., Reilly, T.H., Bruegge, C.J., Conel, J.E., Martonchik, J.V., Ackerman, T.P., Davies, R., Gerstl, S.S.W., Gordon, H.R., Muller, J.-P., Myneni, R., Seller, R.J., Pinty, B. and Verstraete, M.M., 1998, Multiangle Imaging SpectroRadiometer (MISR) description and experiment overview. *IEEE Transactions on Geoscience and Remote Sensing*, **36**, pp. 1072–1087.

Diner, N.L., Beckert, J.C., Bothwell, G.W. and Rodriguez, J.I., 2002, Performance of the MISR instrument during its first 20 months in Earth orbit. *IEEE Transactions on Geoscience and Remote Sensing*, **40**, pp. 1449–1466.

Esaias, W.E., Abbott, M.R., Barton, I., Brown, O.W., Campbell, J.W., Carder, K.L., Clark, D.K., Evans, R.L., Hoge, F.E., Gordon, H.R., Balch, W.P., Letelier, R. and Minnett, P.J.,1998, An overview of MODIS capabilities for ocean science observations. *IEEE Transactions on Geoscience and Remote Sensing*, **36**, pp. 1250–1265.

Esposito, J., Xiong, X., Wu, A., Sun, J. and Barnes, W.L., 2004, MODIS reflective solar bands calibration uncertainty analysis. *Proceedings of SPIE – Earth Observing Systems IX*, **5542**, pp. 448–456.

Guenther, B., Xiong, X., Salomonson, V.V., Barnes, W.L. and Young, J., 2002, On-orbit performance of the Earth Observing System (EOS) Moderate Resolution Imaging Spectroradiometer (MODIS) and the attendant Level 1-B data product. *Remote Sensing of the Environment*, **83**, pp. 16–30.

Justice, C.O., Vermote, E., Townshend, J.R.G., DeFries, R., Roy, D.P., Hall, D.K., Salomonson, V.V., Privette, J.L., Riggs, G., Strahler, A., Lucht, W., Myneni, R.B., Lewis, P. and Barnsley, M.J., 1998, The Moderate Resolution Imaging Spectroradiometer (MODIS): land remote sensing for global change research. *IEEE Transactions on Geoscience and Remote Sensing*, **36**, pp. 1228–1249.

King, M. and Greenstone, R. (Eds.), 1999, *NASA EOS Reference Hand Book: A Guide to Earth Science Enterprise and the Earth Observation Systems* (Greenbelt, MD: EOS Project Science Office, NASA/Goddard Space Flight Center).

King, M.D., Menzel, W.P., Kaufman, Y.J., Tanre, D., Gao, B.C., Platnick, S., Ackerman, S.A., Remer, L.A., Pincus, R. and Hubanks, P.A., 2003, Cloud and aerosol properties, precipitable water, and profiles of temperature and humidity from MODIS. *IEEE Transactions on Geoscience and Remote Sensing*, **41**, pp. 442–458.

Kwiatkowska, E.J., Franz, B.A., Meister, G., McClain, C.R. and Xiong, X., 2008, Cross calibration of ocean-color bands from Moderate Resolution Imaging Spectroradiometer on Terra Platform. *Applied Optics*, **47**, pp. 6796–6810.

Moody, E.G., King, M.D., Platnick, S., Schaaf, C.B. and Gao, F., 2005, Spatially complete global spectral surface albedos: value-added datasets derived from Terra MODIS land products. *IEEE Transactions on Geoscience and Remote Sensing*, **43**, pp. 144–158.

Rao, C.R.N. and Chen, J., 1999, Revised post-launch calibration of the visible and near-infrared channels of the Advanced Very High Resolution Radiometer on the NOAA-7, -9, and -11 spacecraft. *International Journal of Remote Sensing*, **20**, pp. 3485–3491.

Salomonson, V.V., Barnes, W.L., Maymon, P., Montgomery, H. and Ostrow, H., 1989, MODIS: advanced facility instrument for studies of the Earth as a system. *IEEE Transactions on Geoscience and Remote Sensing*, **27**, pp. 145–153.

Sun, J., Xiong, X., Barnes, W.L. and Guenther, B., 2007, MODIS reflective solar bands on-orbit lunar calibration. *IEEE Transactions on Geoscience and Remote Sensing*, **45**, pp. 2383–2393.

Sun, J., Xiong, X., Guenther, B. and Barnes, W.L., 2003, Radiometric stability monitoring of the MODIS reflective solar bands using the Moon. *Metrologia*, **40**, pp. 85–88.

Thome, K., Markham, B., Barker, J., Slater, P. and Biggar, S., 1997, Radiometric calibration of Landsat. *Photogrammetric Engineering and Remote Sensing*, **63**, pp. 853–858.

Wu, A., Cao, C. and Xiong, X., 2003, Inter-comparison of 11 μm and 12 μm bands of Terra and Aqua MODIS using NOAA-17 AVHRR. *Proceedings of SPIE – Earth Observing Systems VIII*, **5151**, pp. 384–394.

Wu, A., Xiong, X. and Cao, C., 2008, Terra and Aqua MODIS inter-comparison of three reflective solar bands using AVHRR onboard the NOAA-KLM satellites. *International Journal of Remote Sensing*, **29**, pp. 1997–2010.

Xiong, X. and Barnes, W.L., 2006, An overview of MODIS radiometric calibration and characterization. *Advances in Atmospheric Sciences*, **23**, pp. 69–79.

Xiong, X., Barnes, W.L. and Murphy, R.E., 2003a, Lessons learned from MODIS calibration and characterization. *Journal of Advances in Space Research*, **32**, pp. 2017–2122.

Xiong, X., Che, N., Pan, C., Xie, X., Sun, J., Barnes, W.L. and Guenther, B., 2006, Results and lessons from MODIS reflective solar bands calibration: pre-launch to on-orbit. *Proceedings of SPIE – Earth Observing Systems XI*, **6296**, doi:10.1117/12.679144.

Xiong, X., Chiang, K., Guenther, B., and Barnes, W.L., 2002a, MODIS thermal emissive bands calibration algorithm and on-orbit performance. *Optical Remote Sensing of the Atmosphere and Clouds III, Proceeding of SPIE*, **4891**, pp. 392–401.

Xiong, X., Sun, J., Barnes, W.L., Salomonson, V.V., Esposito, J., Erives, H. and Guenther, B., 2007, Multiyear on-orbit calibration and performance of Terra MODIS reflective solar bands. *IEEE Transactions on Geoscience and Remote Sensing*, **45**, pp. 879–889.

Xiong, X., Sun, J., Chiang, K., Xiong, S. and Barnes, W.L., 2003b, MODIS on-orbit characterization using the Moon. *Proceedings of SPIE – Sensors, Systems, and Next Generation Satellite VI*, **4881**, pp. 299–307.

Xiong, X., Wu, A. and Angal, A., 2008a, Assessment of MODIS scan mirror reflectance changes on-orbit. *SPIE – Earth Observing Systems XIII*, **7081**, pp. 7081–7089.

Xiong, X., Wu, A. and Cao, C., 2008b, On-orbit calibration and inter-comparison of Terra and Aqua MODIS surface temperature spectral bands. *International Journal of Remote Sensing*, **29**, pp. 5347–5359.

Xiong, X., Wu, A., Esposito, J.A., Sun, J., Che, N., Guenther, B. and Barnes, W.L., 2002b, Trending results of MODIS optics on-orbit degradation. *Proceedings of SPIE – Earth Observing Systems VII*, **4814**, pp. 337–346.

Xiong, X., Wu, A. and Wenny, B., 2008c, Using Dome C for MODIS calibration and characterization. *Proceedings of SPIE – Sensors, Systems, and Next Generation Satellites XII*, **7106**, pp. 7106–7131.